Physics and engineering design of the Accelerator and Electron Dump for SPIDER

P. Agostinetti[a], V. Antoni[a], M. Cavenago[b], G. Chitarin[a], N. Marconato[a], D. Marcuzzi[a], N. Pilan[a], G. Serianni[a], P. Sonato[a], P. Veltri[a], P. Zaccaria[a]

[a] *Consorzio RFX, Euratom-ENEA Association, C.so Stati Uniti 4, I -35127, Padova, Italy*
[b] *INFN, Laboratori Nazionali di Legnaro, v.le dell'Universita' 2, 35020 Legnaro, Italy*

Abstract

The ITER Neutral Beam Test Facility (PRIMA) is planned to be built at Consorzio RFX (Padova, Italy). PRIMA includes two experimental devices: a full size ion source with low voltage extraction called SPIDER and a full size neutral beam injector at full beam power called MITICA. SPIDER is the first experimental device to be built and operated, aiming at testing the extraction of a negative ion beam (made of H^- and in a later stage D^- ions) from an ITER size ion source. The main requirements of this experiment are a H^- / D^- extracted current density larger than 355 / 285 A m^{-2}, an energy of 100 keV and a pulse duration of up to 3600 s.

Several analytical and numerical codes have been used for the design optimization process, some of which are commercial codes, while some others were developed ad hoc. The codes are used to simulate the electrical fields (SLACCAD, BYPO, OPERA), the magnetic fields (OPERA, ANSYS, COMSOL, PERMAG), the beam aiming (OPERA, IRES), the pressure inside the accelerator (CONDUCT, STRIP), the stripping reactions and transmitted/dumped power (EAMCC), the operating temperature, stress and deformations (ALIGN, ANSYS) and the heat loads on the electron dump (EDAC, BACKSCAT).

An integrated approach, taking into consideration at the same time physics and engineering aspects, has been adopted all along the design process. Particular care has been taken in investigating the many interactions between physics and engineering aspects of the experiment. According to the "robust design" philosophy, a comprehensive set of sensitivity analyses was performed, in order to investigate the influence of the design choices to the most relevant operating parameters.

The design of the SPIDER accelerator, here described, has been developed in order to satisfy with reasonable margin all the requirements given by ITER, from the physics and engineering points of view. In particular, a new approach to the compensation of unwanted beam deflections inside the accelerator and a new concept for the Electron Dump have been introduced.

1. Introduction

In the framework of the activities aimed at developing and optimizing the Heating and Current Drive Neutral Beam Injectors (H&CD NBIs) for ITER [1, 2], the SPIDER (Source for Production of Ion of Deuterium Extracted from RF plasma) and MITICA (Megavolt ITER Injector Concept Advancement) experiments are planned to be built at Consorzio RFX in the PRIMA (Padova Research on Injector Megavolt Accelerated) facility. The main requirements of SPIDER are a H^- / D^- extracted current density larger than 355 / 285 A m^{-2}, a particle energy of 100 keV and a pulse duration up to 3600 s.

An ITER size Radio Frequency (RF) Ion Source is foreseen for the SPIDER experiment, whose design is based on the R&D carried out at IPP Garching [3, 4, 5, 6].

A first version of the SPIDER accelerator design was presented in 2008 [7, 8, 9]. Since then, further studies have been carried out by the RFX team: the magnetic configuration has been modified in order to ensure good beam optics and aiming, and a new component - the Electron Dump (ED) - has been added in order to dump the electrons exiting the accelerator. This paper describes the physics and engineering design of the accelerator and electron dump for SPIDER.

2. Design description

The extraction and accelerator system for the SPIDER ion source, sketched in Fig. 1, is composed of three grids: the Plasma Grid (PG), the Extraction Grid (EG) and the Grounded Grid (GG). The grids are approximately 1600 mm high and 800 mm wide (divided into four segments for alignment and manufacturing reasons). Each grid features 1280 apertures, where the ion beamlets are extracted from the ion source and accelerated up to 100 kV. The SPIDER experiment will have some points in common with the Diagnostic Neutral Beam [10] for ITER (in fact, it has similar requirements on the extracted current and voltages), to be developed and tested by ITER-India.

The PG is heated by the plasma inside the RF-driven ion source, with a surface power density that is estimated to range between 3 and 20 kW m^{-2} (IPP experimental results [4]). Both the ion source and the PG are kept at a potential of -100 kV (with respect to ground) by a dedicated power supply. The PG is required to operate at a temperature of about 150 °C in order to enhance the caesium effect for negative ion surface generation. Moreover, this grid is Molybdenum coated on the plasma side to reduce the sputtering yield, thus prolonging the caesium effect. The apertures are designed with conical chamfers on the upstream and downstream sides of the grid. This solution

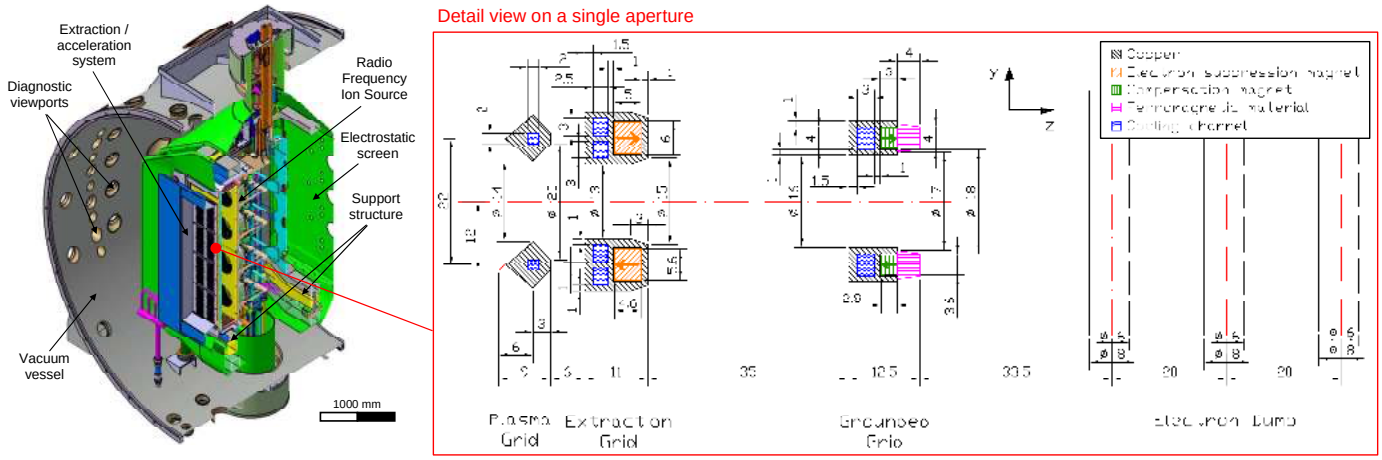

Figure 1: Overall view and Vertical section of the SPIDER extractor/accelerator system and electron dump. All the dimensions are in mm.

provides a wider surface for ion production and a larger probability for ion extraction; its efficacy has been demonstrated by experimental results on the Batman ion source at IPP Garching [3, 11]. A current flows in the vertical direction, to provide a horizontal magnetic field, called "filter field", that reduces the local electron density (and so the number of co-extracted electrons) and the local electron temperature (and so the negative ion stripping rate). A ferromagnetic plate downstream of the GG helps to decrease the magnetic field along the horizontal transverse direction. Details on the optimization of this field are reported in [12].

The EG electric potential is 9 - 10 kV higher than the PG (depending on the extracted current density), so that the negative charged ions (H^- or D^-) can be properly extracted from the RF expansion chamber. The function of the suppression magnets, embedded in the grid, is to deviate the trajectories of the co-extracted electrons, forcing them to collide with the grid surface.

The electric field between the EG and the GG accelerates the ion beamlets up to an energy of about 100 keV. Acceleration of co-extracted and stripped electrons must be minimized in order to reduce power loss and avoid overheating of the grids and other components. The GG also compensates for the beamlet deflections inside the accelerator, as described in the following sections.

All the grids are made by electrodeposition of pure copper onto a copper base plate. This technique permits to obtain a very complex geometric shape (with very small cooling channels that run inside the grid and grooves for embedded magnets) and to have good mechanical properties, due to the high purity and to the very small grain size of copper. The power loads on the EG and GG are expected to be quite high and concentrated, hence they are critical from the structural point of view, and require high performance cooling systems.

2.1. Design improvements

The SPIDER extraction/acceleration system has been improved with respect to the design presented during 2008. In particular, the following actions have been taken:

- The position of the electron suppression magnets in the EG has been changed in order to comply with the updated cooling channels (that were slightly increased in size in order to better satisfy the requirements on the alignment of the grids under operation).

- Compensation magnets and ferromagnetic material have been added in the GG. The position and strength of these magnets, together with the ferromagnetic material, have been tuned in order to provide an effective compensation of the horizontal deflection due to the electron suppression magnets. As a consequence, the GG cooling channel dimensions have been decreased, still satisfying all the thermo-structural requirements.

- The shape of the ferromagnetic material has been optimized in order to reduce the heat loads due to secondary electrons generated downstream of the GG, while maintaining a negligible influence on the vacuum pumping. In particular, the apertures on the iron part of the GG are conical divergent and with a larger diameter than the ones on the copper part of the GG.

- An electron dump (ED) has been added in order to discard the electrons exiting from the accelerator. The ED is composed of a series of vertical pipes (whose axis is aligned with the y direction in Fig. 1) surrounding the apertures and located downstream of the GG. Otherwise, these electrons would be loading the STRIKE calorimeter [13] and the vessel. This component has been optimized in order to provide an effective dumping of electrons escaping from the accelerator, being at the same time compatible with the constraints given by the other components (mainly, geometric and layout constraints).

- The minimum copper thickness of the EG cooling channels has been increased to 1.5 mm (the previous value was 1 mm) in order to have a larger safety factor against water leakage (possible causes can be corrosion or erosion by

water, localized melting or surface sputtering). This modification has also the advantage of a lower out-of-plane deformation of the EG.

3. Single beamlet optics analyses

The goal of the single beamlet optics analyses is to investigate the effect of the main operating parameters (extracted current density and grid voltages) on the optics of the single beamlets, in terms of average divergence. These evaluations are useful both for the design of the SPIDER experiment and for controlling the beam optics during the operations.

The SLACCAD code has been used to estimate the electric field inside the accelerator by integration of the Poisson's equation, with cylindrical geometry conditions [14]. This is a modified version of the SLAC Electron Trajectory Program [15], adapted to include ions, a free plasma boundary and a stripping loss module [16].

The CONDUCT and STRIP codes [17] have been used to generate the boundary conditions for SLACCAD. CONDUCT has been used to estimate the conductance of a gas in low pressure conditions across the aperture, following the classical approach for molecular flow [18]. The temperature of the plasma inside the ion source is foreseen to be around 2000 K [19], while the background gas in the acceleration gaps is expected to be close to the room temperature. Anyway, since the temperature of the plasma inside the ion source could vary during the operations (one of the main goals of SPIDER is to test and optimize the ion source itself), a 300 K temperature have been assumed all along the accelerator in the STRIP code, as a conservative hypothesis. In fact, the assumption of an higher temperature in the ion source would have given lower stripping losses, with consequent lower heat loads on the grids and ED. Using these data as input together with the source and tank pressure (fixed at respectively 0.3 and 0.05 Pa), STRIP has been used to estimate the pressure profile and stripping percentage on beam axis (considering the cross sections reported in the ORNL Redbooks [20]). The stripping and charge exchange reactions have been then taken into account by SLACCAD for the space charge evaluations.

The H^- current density (j_{nom}) required to be extracted from the SPIDER ion source is 355 A m^{-2}, as indicated in Table 2.1 of the System Requirement Document on the Neutral Beam Test Facility [21]. The optics optimization is here reported only for an H^- beam, being the operations with 285 A m^{-2} of D^- similar to 355 A m^{-2} of H^- in terms of optics, taking into account the larger stripping losses of D^-. In fact, the stripping losses with D^- are expected to be slightly higher due to the lower velocity of the D^- particles (at the same energy) that implies a higher cross section for stripping and charge exchange reactions.

According to the "robust design" philosophy [22], the influence of variations on the most relevant operating parameters has been considered. Hence, a set of analyses have been performed with the SLACCAD code considering different possible operating scenarios, in addition to the nominal parameters corresponding to the requirements. This approach leads to a

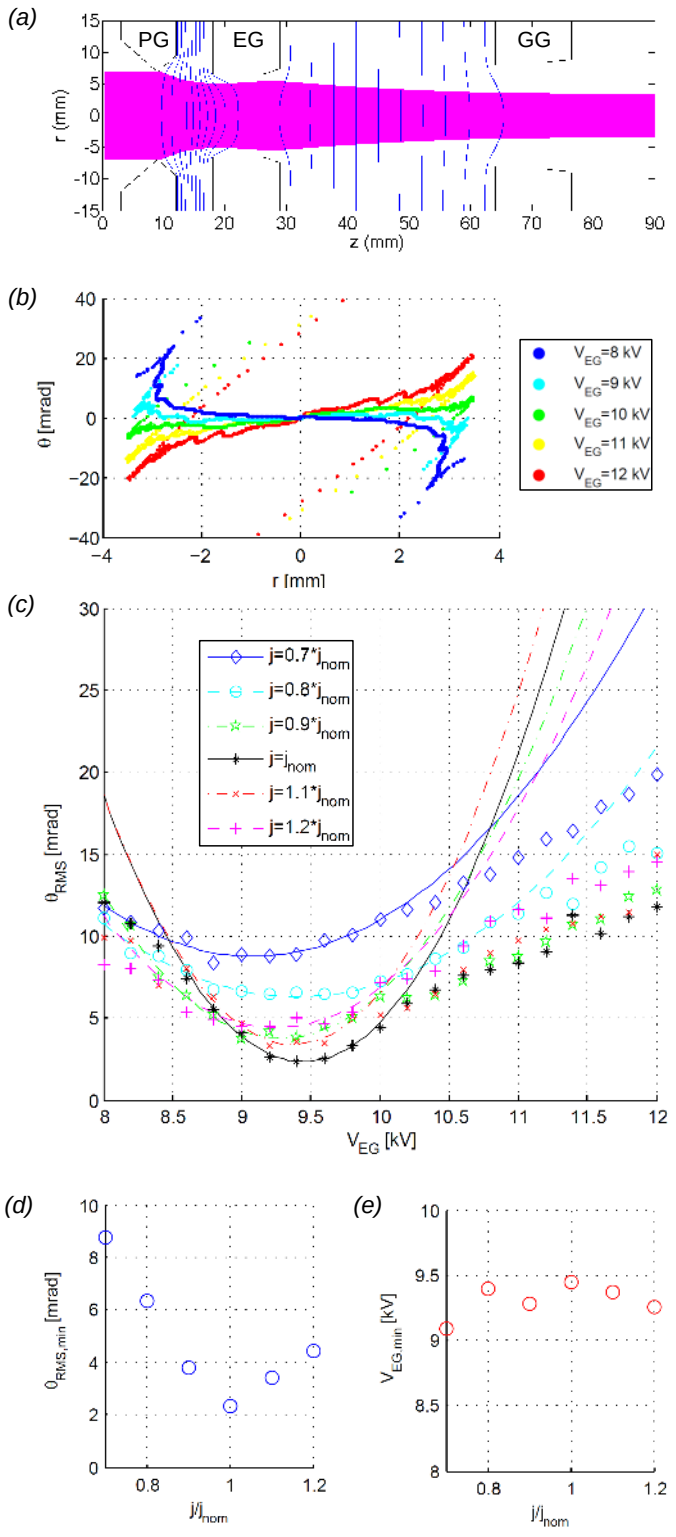

Figure 2: Beam optics analyses with SLACCAD: (a) Trajectories and equipotential lines in the reference conditions ($j = j_{nom}$, V_{PG}=0 kV, V_{EG}=9.4 kV and V_{GG}=100 kV); (b) Divergence angle of the beamlet at the accelerator exit in function of the distance from the beamlet centre, with nominal current and different EG voltage (V_{PG}=0 kV and V_{GG}=100 kV); (c) Sensitivity of θ_{RMS} on EG potential and extracted current (only the points close to the minimum are considered for the interpolating second degree polynomial curves); (d) Minimum θ_{RMS} in function of the extracted current density; (e) EG voltage corresponding to the minimum.

better general knowledge of the system, and can make the optimization process more effective. In particular, a sensitivity analysis has been carried out in order to investigate the influence of the main design parameters (aperture geometry, gaps among the grids, grid potentials and extracted current densities) on the single beamlet optics (with a particular focus on the beamlet divergence, that has been taken as main output parameter). In order to obtain a suitably precise solution and a good convergence of the code, 400 rays have been considered in the simulations of a single beamlet.

Beam optics has been simulated by taking into account the effect of the beamlet space charge, and its reduction due to stripping and charge exchange reactions along the accelerator (estimated with STRIP). The positive ions that are generated inside the accelerator are subjected to the electrical fields, so that their role regarding space charge is neglected; on the other hand, positive ions are foreseen to give a space charge compensation effect outside the accelerator (where there are no electrical fields) starting from a plane 20 mm downstream of the GG [23].

Taking as fixed parameters the PG and GG potentials (respectively 0 and 100 kV), the particle trajectories in axis-symmetrical conditions have been calculated for several combinations of extracted current densities (j) and EG potential (V_{EG}). In Fig. 2b, the divergence angle of the particles is plotted as a function of the distance from the beamlet centre, at nominal current. When the plot is mainly in the first and third quadrant (angle and radius with the same sign), the beamlet is on average divergent, while when it is in the second and fourth quadrant (angle and radius with different signs) the beamlet is on average convergent. It can be observed that while raising the V_{EG}, the beamlet passes from a convergent (corresponding to an over-focussed beamlet) to a divergent shape (under-focussed beamlet). Hence, for each extracted current density, an optimal condition exists between convergence and divergence, where the beamlet is the closest to a cylindrical shape (well focussed beamlet). This condition corresponds to the minimum of the average divergence angle. In order to find this minimum, the root mean square value of the divergence angle θ_{RMS} has been plotted against the EG potential and in function of the extracted current density (see Fig. 2c).

The adopted design permits to obtain the minimum beamlet divergence in a large range of operating scenarios (in particular, strong variations of the extracted current density), by tuning the EG potential. Namely, modifying the relative strength of the various convergent and divergent lenses along the beam path, an optimal condition, corresponding to the minimum θ_{RMS}, can be found for all the extracted current densities in the range 70% - 120% of the nominal value (see Figs. 2d and 2e). In particular, the minimum θ_{RMS} for the nominal extracted current is found to be 2.2 mrad, reached with V_{EG} =9.4 kV. These are considered acceptable reference operating conditions for SPIDER.

4. Multi beamlet optics analyses

Inside a negative ion accelerator, there are generally three main factors that can cause deflection of the ion beamlets: the deformation of the grids under thermal loads, the repulsion among beamlets and the suppression magnetic field. These effects are generally considered detrimental for the ITER NBI, as they are expected to cause higher heat loads on the ITER NBI neutralizer and decrease the overall beam quality (in terms of aiming and divergence). Hence the ion deflection should be considered and minimized also for the SPIDER device, where it will be possible to precisely investigate the beamlet footprint using an instrumented calorimeter relatively close to the accelerator exit [13]. A design optimization process has been carried out aiming at compensating these effects [24]. The OPERA-3D code [25] has been used as the main tool for this optimization process, as it can take into account the beamlet repulsion and the interactions among beamlets and grids. This is made by solving the electrostatic Poisson's equation with a finite element approach, to calculate the particle trajectories of the negative ions under the influence of electrostatic fields, magnetic fields and space charge.

Also the IRES code (Ion Relativistic Equation Solver), developed at Consorzio RFX [26], has been used to simulate the interaction among beamlets, modeling each beamlet as a single particle. The results are found in good agreement with OPERA-3D.

4.1. Effect of aperture offset

Inside an electrostatic accelerator, the position of grid apertures can influence the direction of the beamlets. Investigations on this aspect have been carried out in Germany by Spädtke et al. [27, 28] in UK by Holmes et al. [29], in Japan by the JAERI team [30, 31, 32, 33] and by the NIFS team [34, 35, 36, 37]. Analytical and numerical models, able to simulate the interaction between positive or negative ion beams due to the space charge, were introduced taking into account the boundary conditions corresponding to different experiments.

Regarding SPIDER, a single aperture model and two multi aperture models were developed with the OPERA-3D code (see Fig. 4a). The single aperture model has been used to estimate the deflection of a beamlet due to a possible misalignment among the corresponding apertures of the three grids of the SPIDER extractor/accelerator system. The beamlet has been simulated by launching a large number of macroparticles (representing and ensemble of hydrogen negative ions) from a suitable emitter surface (generated with a dedicated macro) reproducing the meniscus shape calculated by the SLACCAD code in cylindrical symmetry. The macroparticles are then accelerated by the electrical fields applied by the grids, and at the same time they interact among each other (i.e. the repulsion due to space charge is taken into account). The electrical potential in every point is iteratively calculated by solving the Poisson's equation in a 3D domain.

In the presence of a deliberate or accidental offset among the aperture axes, due to the curved shape of the equipotential surfaces, the beamlet is deflected. In fact, there are two field curvatures inside the EG: one concave at the upstream side (close to the PG-EG gap) and a second convex one at the downstream side (close to the EG-GG gap), as can be seen in Fig. 3a. Due to the fact that the electrical field in the second gap is stronger

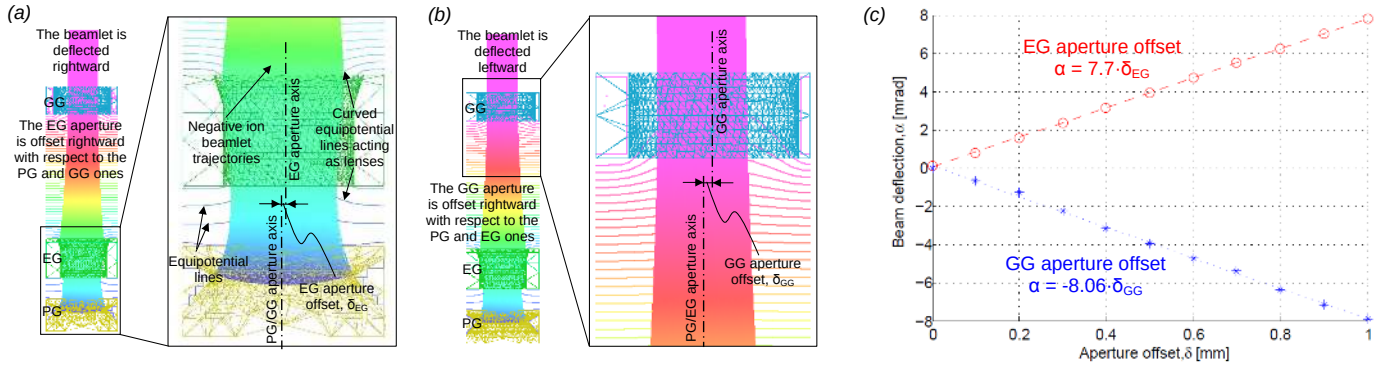

Figure 3: Analysis of the effect of misalignment among corresponding apertures on the three grids, estimated with OPERA-3D: (a) Effect of an EG aperture offset; (b) Effect of a GG aperture offset; (c) Correlation between aperture offset and beamlet deflection. The PG, EG and GG potentials are respectively at 0, 9.4 and 100 kV.

than the one in the first, if the EG aperture is shifted rightwards, the average deflection given by the second curvature prevails on the one given by the first one, so there is a residual deflection effect rightward. As there is no field downstream of the GG, only a concave curvature exists inside this grid at the upstream side (see Fig. 3b). Hence, when for example the GG aperture is offset rightward, the beamlet is deflected leftward.

The results of a set of analyses, carried out to find a correlation between the aperture offsets and the beamlet deflection, are summarized in Fig. 3c. If there is a misalignment among the apertures on the three grids (caused for example by non-nominal thermal loads on the grids) the correlated beamlet deflection can be estimated from the interpolating equations (reported in Fig. 3c). On the other hand, if there are deflections due to other causes (space charge or magnetic field), they can be compensated for by proper offsets deliberately applied to the apertures.

4.2. Compensation for beam deflections

In general, we have found that, in order to compensate for an unwanted effect on ion optics (such as the deflection given by the suppression magnets and the repulsion among beamlets), it is more efficient to act directly on the cause that has generated this effect, rather than on other factors. In this way, the compensation is more robust even for operating conditions far from the reference values (for example, with half extracted current density); such conditions could be likely during the experimental campaigns.

Following this strategy, an aperture offset (compensation by electrical field adjustment) has been exploited for the compensation of the repulsion among beamlets, that is essentially an electric field interaction.

Analogously, the ion beam deflection due to the electron suppression magnets in the EG is better compensated using magnetic fields rather than electrostatic fields. Therefore, compensating magnets have been adopted rather than aperture offsets. In this way, the compensation is effective in a wide range of operating scenarios, while in the other way it would be limited to the reference grid voltages and extracted current.

4.2.1. Compensation of the beamlet deflection given by the repulsion among beamlets

The repulsion among ion beamlets causes a transverse outward deflection, which is negligible for the beamlets located close to the centre of each aperture group and maximum for those located at the peripheral apertures, with a consequent increase of the overall divergence of the beam. Two possible design modifications for the compensation for the repulsion among beamlets were identified:

1. the introduction of a mechanical offset of the GG apertures;
2. the introduction of kerbs on the downstream side of the EG.

The former solution has been chosen for SPIDER, because the latter one might increase the risk of discharges between EG and GG. An horizontal array model (with 5x1 apertures, see Fig. 4a) has been used to estimate the beamlet deflection due to the repulsion among 5 adjacent beamlets. Parallel electrical field boundary conditions are applied to the four domain borders parallel to the beamlet axis. Half of the region between two aperture groups is simulated at the left and right sides of the aperture array. As shown in Fig. 4b, the external beamlets are deflected outwards. In particular the first and the fifth beamlets present a deflection of 2.4 mrad, while the second and fourth are deflected by about 0.5 mrad. These deflections are evaluated by calculating the average value of the horizontal deflection of the macroparticle trajectories at the accelerator exit. A set of analyses has been also performed using models with 10x1 and 1x32 apertures (respectively doubling the 5x1 and 1x16 models shown in Fig. 4a), showing that the repulsion among adjacent 5x16 beamlet groups is negligible.

In order to compensate for the deflection due to the repulsion among beamlets, a proper mechanical offset has been sought for the apertures 1,2,4 and 5. As shown in Fig. 3, both EG and GG aperture offsets can deflect the beamlets. Nevertheless, offsetting the EG aperture seems not advisable, as the tolerance between the beamlet and grid aperture is quite small at the EG and the beamlet would risk to collide with the aperture internal surface, as visible in Fig. 3. Such an event would cause spoiled

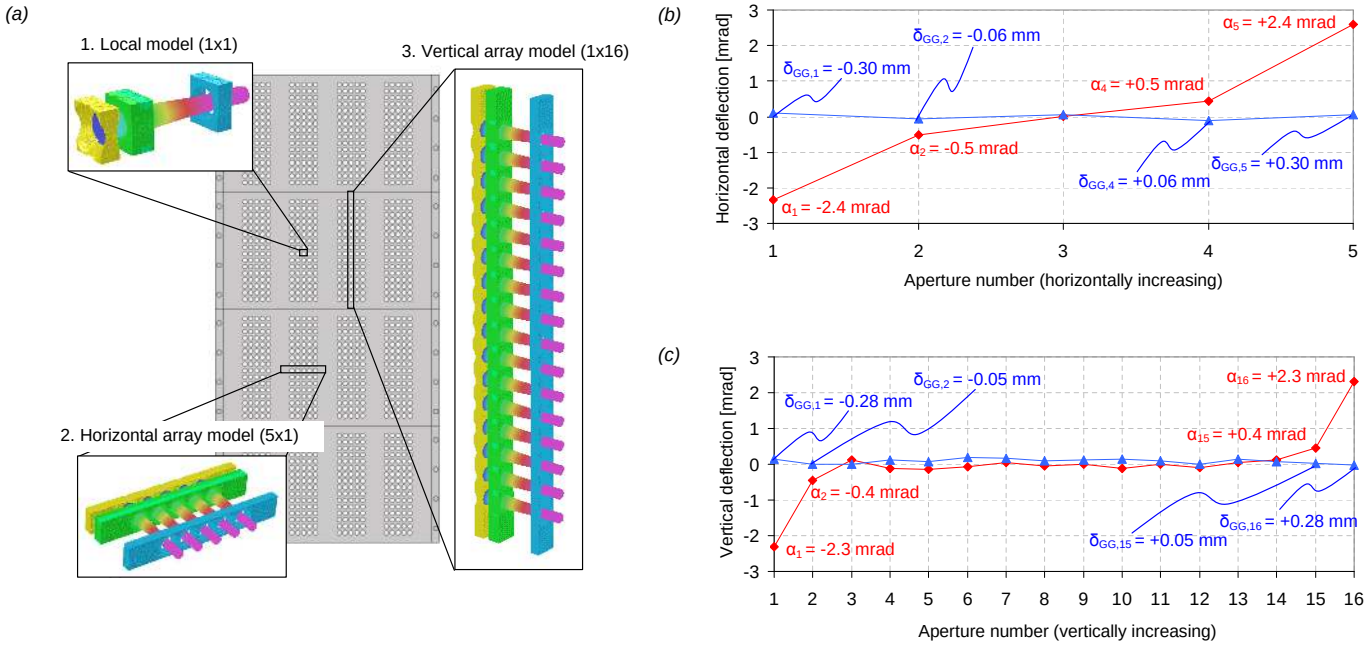

Figure 4: Evaluation with OPERA-3D of the repulsion among beamlets and its compensation: (a) Models of the SPIDER extractor/accelerator system used for the investigations on beam optics and aiming; (b) Horizontal deflection compensation; (c) Vertical deflection compensation. The red dots represent the beamlet deflections due to the repulsion among beamlets; deflections angles for each beamlet are reported in red. The blue dots represent the beamlet deflections after introducing proper offsets to the GG apertures, that compensate for the repulsion among beamlets; the optimized values of the aperture offsets are reported in blue.

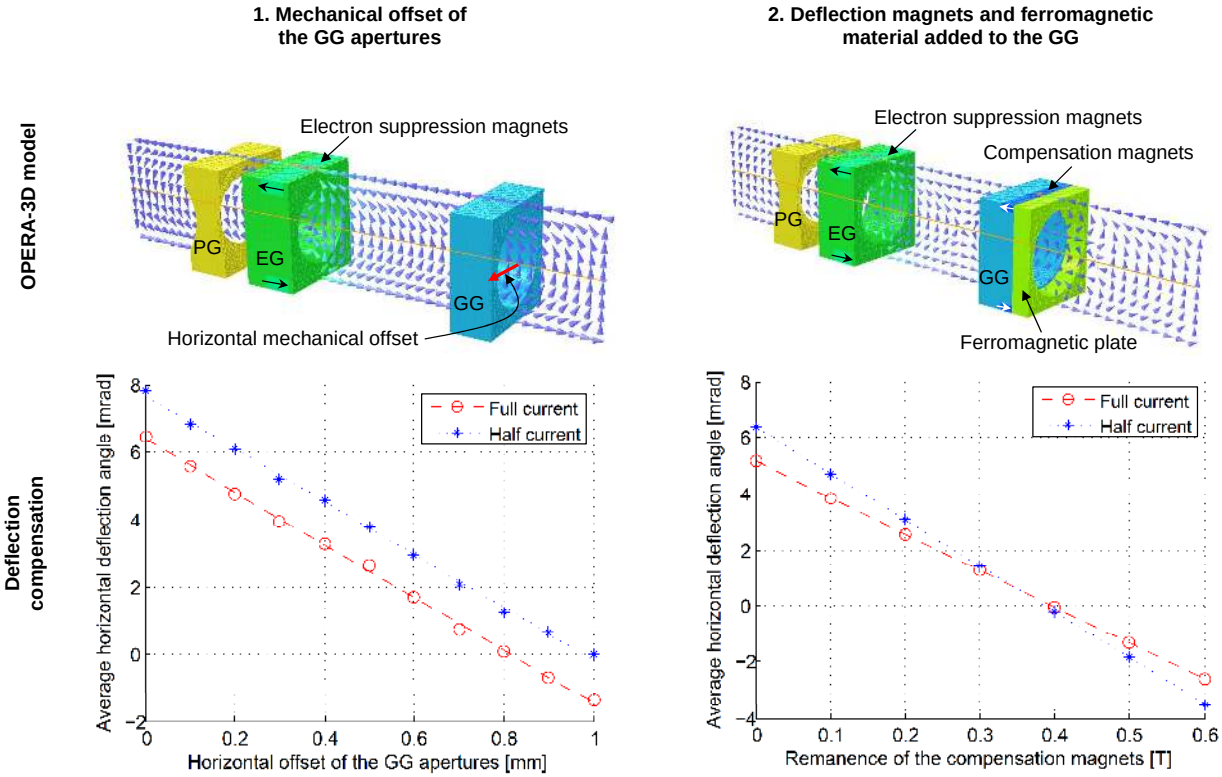

Figure 5: Evaluation with OPERA-3D of two approaches for the compensation of the deflection given by the electron suppression magnets.

beam optics, increase of secondary electrons and highly concentrated heat loads (with a consequent risk of localized melting). On the other hand, at the GG the aperture internal surface is not so close to the beamlet, because the beamlet itself has a smaller diameter and the GG aperture diameter is larger than the EG one. Consequently, it appears safer to apply an aperture offset to the GG than to the EG. Moreover, the steering constant of the GG aperture is almost independent of the extraction voltage chosen, whereas the steering constant of the EG aperture depends strongly on it. The proper values for the offsets have been calculated with the inverse of the GG offset equation reported in Fig. 3c (resulting from the OPERA calculations):

$$\delta_{GG} = -\frac{\alpha}{8.06} \tag{1}$$

where α is the deflection in mrad and δ_{GG} is the GG aperture offset in mm. By applying this mechanical offset to the GG aperture, the repulsion effect has been found to be completely compensated. This is visible in Fig. 4b, where the applied offsets are reported in blue.

A similar method has been applied for the compensation of the repulsion among beamlets in the vertical direction. First of all, an analysis with zero aperture offset has been carried out using a vertical array model (1x16, see Fig. 4a). The results show that the two upper and two lower beamlets are deflected respectively upward and downward. Then, the proper offsets to be applied in order to compensate for the repulsion have been calculated with Eq. (1), analogously to the horizontal direction. After introducing these offsets to the GG apertures of the involved beamlets (1,2,15 and 16), also the vertical repulsion has been compensated (see Fig. 4c). Based on these results, the following outward offsets are to be applied in order to cancel the effect of the repulsion among beamlets in a 5x16 beamlet group:

- the GG apertures columns 1 and 5 must be offset by 0.30 mm;
- the GG apertures columns 2 and 4 must be offset by 0.06 mm;
- the GG apertures rows 1 and 16 must be offset by 0.28 mm;
- the GG apertures rows 2 and 15 must be offset by 0.05 mm.

4.2.2. Compensation of the beamlet deflection given by the suppression magnetic field

The magnetic field given by the electron suppression magnets in the EG has the function to deflect the electrons which are extracted from the ion source to make them impinge on the EG itself (see for example Fig. 6b). According to the design, these magnets will have a section of 5.6 x 4.6 mm^2, and shall be inserted in slots with sections 6 x 5 mm^2 (see Fig. 1). After a survey on the market, Sm_2Co_{17} was chosen for these magnets. This material, able to reach a magnetic remanence up to 1.1 T and a continuous operating temperature up to 350 °C, was preferred to $SmCo_5$, $Nd_2Fe_{14}B$ and Alnico because of its higher performances in terms of remanence, energy density and magnetization stability at high temperature.

The suppression magnetic field induces a deflection also of the negative ions. As the polarities of the magnets are alternated from row to row, the beamlet deflection is also alternated, causing a vertical ripple effect.

Two possible approaches have been considered for the compensation of this detrimental effect (see Fig. 5):

1. to introduce a further mechanical offset of the GG apertures;
2. to introduce a compensating magnetic field, by means of compensation magnets and ferromagnetic material in the GG.

It can be observed from Fig. 5 that the deflection due to the suppression magnetic field changes depending on the extracted current density (half or full current). This is due to the fact that, if the extracted current density is varied, for an acceptable beam optics also the grid voltages must be varied, so that the optimal perveance match can be maintained for each acceleration gap (by keeping the same ratio between the extracted current and the potential difference elevated to the power of 3/2). In order to compensate for this deflection with the first approach, the GG apertures must be offset by 0.8 mm (see the left part of Fig. 5). Nevertheless, the compensation is complete only at full current, while it is only partial at half current.

The second approach for the compensation of the deflection given by the suppression magnetic field relies on magnets and ferromagnetic material in the GG. Several analyses have been carried out in order to tune the compensation magnets and the ferromagnetic material in the GG for an optimal compensation of the beam deflection given by the suppression magnets. Taking into account all the constraints, the compensation magnets have been designed with a section of 3.6 x 2.8 mm^2 and with a magnetic remanence of 0.4 T (obtainable with magnets made of hard ferrite), and the ferromagnetic plate (soft iron, μ=1000) with a thickness of 4 mm. The effect of this compensation magnetic field is shown in Fig. 5 on the right.

The maximum $|B|$ inside the ferromagnetic plate is about 0.54 T, which is to be considered acceptable (saturation is at about 1 T for soft iron). Only the magnetic field by suppression and compensation magnets are considered in these simulations, while the filter field is neglected. The filter field is so small that it will not interact in the ferromagnetic material regarding saturation effects.

It can be observed from Fig. 5 that:

- The solution based on GG offset loses effectiveness if the extracted current is different from the nominal one. Moreover, this is a rigid solution (not modifiable without changing the whole GG). This is to be thought of as a weakness of this solution if we consider that the estimations of the beam deflection are affected by some uncertainties and haven't been experimentally validated so far.
- The solution based on compensating magnets in the GG should work efficiently also with an extracted current different from the nominal one. Moreover, it is expected to

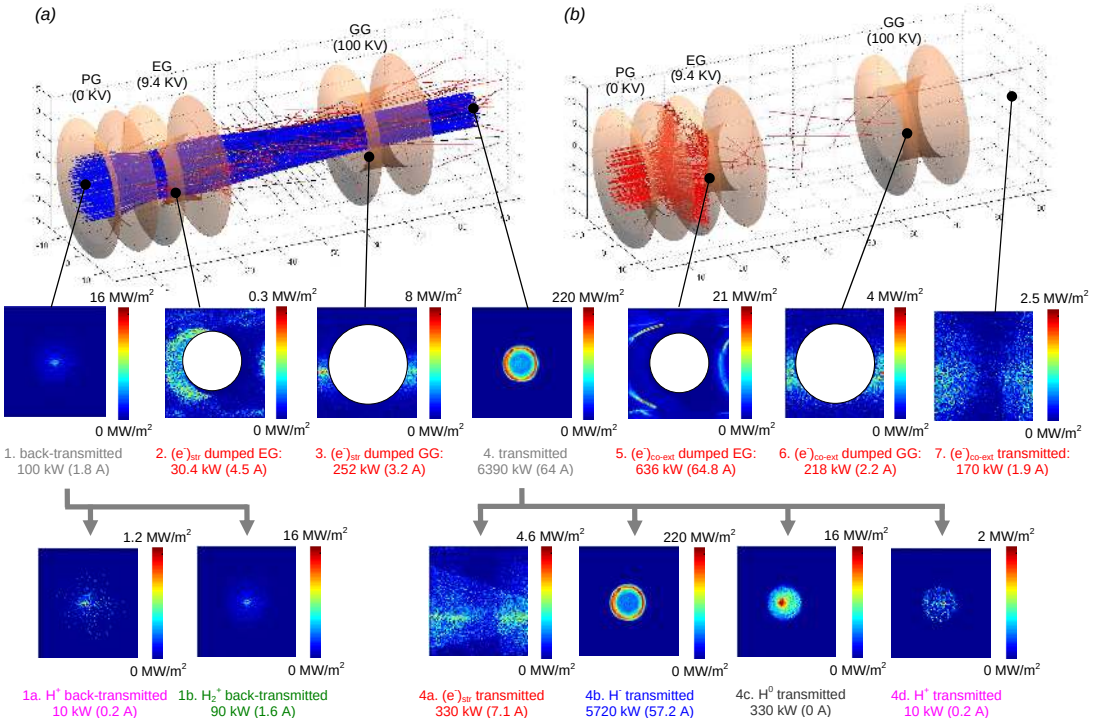

Figure 6: EAMCC simulation (a) of a negative ion beamlet and (b) of the co-extracted electrons in the SPIDER accelerator: the particle trajectories and stripping reactions are simulated with a Monte Carlo approach in a domain with electrical and magnetic fields. The power loads and currents corresponding to the whole accelerator (1280 beamlets) are reported.

be more flexible. In fact, it is possible to change the compensation magnets in the GG and/or the thickness of the ferromagnetic plate without changing the GG.

For these reasons, in accordance with the general strategy described in the previous paragraph, the second approach has been chosen for the design.

5. Estimation of the heat loads on the grids and of dumped/transmitted particles

The collisions among particles inside the accelerator, as well as secondary particle production processes, were analysed with the EAMCC code. This is a 3-dimensional relativistic particle tracking code where macroparticle trajectories, in prescribed electrostatic and magnetostatic fields, are calculated inside the accelerator [38, 39]. In the code, each macroparticle represents an ensemble of rays considering the time-independent physical characteristics of the system. This code needs as inputs the electric and magnetic fields inside the accelerator.

Collisions are described using a Monte-Carlo method. The collisions considered in the code are the ones between the particles (electrons, ions and neutrals) and the grids, the negative ion single and double stripping reactions and the ionization of background gas. The main parameters used for the EAMCC simulations are:

- Extracted H^- current density: 355 A/m^2, as required by ITER [21].
- Extracted e^- current density: 355 A/m^2; the extracted e^-/H^- ratio is assumed equal to 1, for safety reasons, though ITER requires a value lower than 0.5 [21]. The experience at IPP Garching indicates that low values of the extracted e^-/H^- ratio (1 or less) can be obtained only with a good distribution of caesium inside the ion source [40, 41]; during the conditioning phase, this ratio is usually higher, with consequent higher heat loads on the grids than with the optimal operating conditions.
- Electrostatic field: evaluated with SLACCAD in cylindrical geometry (see Par. 3); the results of these electrostatic calculations have been compared with the electrostatic field computed by the BYPO code [42] in slab geometry, with fair agreement considering the different symmetry conditions [9].
- Magnetic field: suppression/compensation magnetic field was evaluated with OPERA (optimized to compensate for deflection, see Par. 4). The filter field [12] and the full 3D magnetic model of the accelerator (including edge effects) [43] were developed in ANSYS. The results of the magnetic calculations have been compared among the codes OPERA [25], ANSYS [44], COMSOL [45] and PERMAG [46], with very good agreement.
- Pressure profile: from STRIP, considering a pressure of 0.3 Pa inside the RF source and of 0.05 Pa downstream of the GG;

- Gas temperature at the emitter: 0.18 eV (corresponding to approximately 2000 K, as measured in the BATMAN source at IPP [19]).

Fig. 6 shows the main results of the EAMCC calculations. The trajectories of negative ions and of electrons for a single SPIDER beamlet are shown. Two separate simulations are performed to simulate the H^- ions (and related species generated by stripping) and the co-extracted electrons. The thermal load around the apertures and the transmitted power are also indicated. The current density is assumed to be the same (355 A m^{-2}) in the two cases, considering an extracted e^-/H^- ratio of 1. The heat loads on the grid surfaces are evaluated by summing the two contributions.

The transmitted beamlet power density at the accelerator exit features a ring that is hotter than the central part. This effect is not observed if the downstream surface of the PG is flat, i.e. without the diverging conical chamfers, which are anyway required on account of Pierce's considerations [47].

The backstreaming positive ions are quite concentrated in the center of the aperture area. The consequent heat power density is quite high, but covers only an area of some tens of square millimeters. These ions could give rise to sputtering phenomena on the plasma source back plate and on the driver Faraday shields, with a consequent decay of the plasma purity and problems of surface integrity. The sputtering yield due to the backstreaming ions is generally reduced by a factor of about 5 if the copper surface is coated with Molybdenum. Hence, in order to minimize the detrimental effects consequent to sputtering, a layer of Molybdenum of some microns is foreseen to be applied on the plasma source back plate.

6. Electron dump design

A power of about half a MW is carried by the electrons at the accelerator exit, as visible from Fig. 6 (subfigures 4a and 7). Possible ways to dispose of these electrons by means of an electron dump have been investigated in the past. Magnetic fields were proposed to deflect the electrons downwards onto suitably cooled plates: the plates were located at the bottom of the vacuum vessel and at the entrance of the neutraliser; another possibility envisaged four horizontal plates at the exit of the GG [48]. The main disadvantages of such solutions are the large angle with which the particles hit the single electron dump plate (resulting in an energy flux of a few tens of MW/m^2) and the overall dimensions of the multiple plates, which can also be an obstruction for beam diagnostics. Another explored possibility was the horizontal deflection of electrons onto suitable vertical plates. This solution, proposed in [49], could be realised by five electron dump plates (called "blinker" dumps), each one dedicated to a column of four beamlet groups; however it turns out again that the size of the plates is too large for the SPIDER diagnostics requirements. Another possibility consists in the insertion of the electron dump plates in between the beamlet columns: each dump plate receives the power associated to one beamlet only (per row) and the attack angle can be quite small, thus spreading the power over a large surface; moreover the dump plates can be only some centimetres long. Further work has allowed devising a modified solution, in which the vertical plates are substituted by arrays of pipes, distributed so as to intercept most of the electrons.

The ED design has been optimized according to the following requirements:

- The main part (at least 85%) of the total power from accelerated electrons exiting from the GG (co-extracted and stripped) must be dumped by means of the ED.
- All the negative ion beamlets shall pass through the electron dump without being absorbed. This shall be guaranteed up to a beamlet deflection of 15 mrad, being this figure the sum of the maximum deflections if no compensation is working. A safety margin on the beamlet deflection is adopted to allow for:
  - operations in conditions that are different from the nominal ones;
  - approximations in the simulations.

In any case, the power load on the single tubes must be sufficiently low in order to be removed by the water inside the ED tubes so as to have acceptable values of temperature, stress, strain and tube deflections. In particular, this must happen for the first tube array (the closest to the GG) which is the most loaded. Moreover, the power load should be shared as uniformly as possible among the tubes.

6.1. Estimation of the heat load on the electron dump

EDAC (Electron Dump Accountancy Code), a 3D code developed at Consorzio RFX, has been used to estimate the heat load given by the particles exiting the accelerator (electrons, negative ions and neutrals) on the ED. The main operations performed by this code are:

1. importing from EAMCC the accelerator geometry and the position/velocity of the particles (in the reference operating conditions, with $j = j_{nom}$, V_{PG}=0 kV, V_{EG}=9.4 kV and V_{GG}=100 kV) at a plane 20 mm downstream of the accelerator exit (where the space charge is assumed to be completely compensated);
2. extending the trajectories until they hit an ED tube or the target positioned after the ED; periodic conditions are set at the horizontal and vertical boundaries, i.e. if the trajectories are exiting from the boundary, they re-enter from the opposite boundary with the same velocity (this is similarly applied in the EAMCC code);
3. evaluating the power load deposited onto any single micro-area (both the tubes and the target are divided into a customizable number of micro-areas). If the number of trajectories considered is sufficiently high, the power density can be estimated.

As estimated in Par. 5, the power from electrons transmitted beyond the GG for the whole accelerator (1280 beamlets) is ~170 kW from the offspring of the co-extracted electrons and

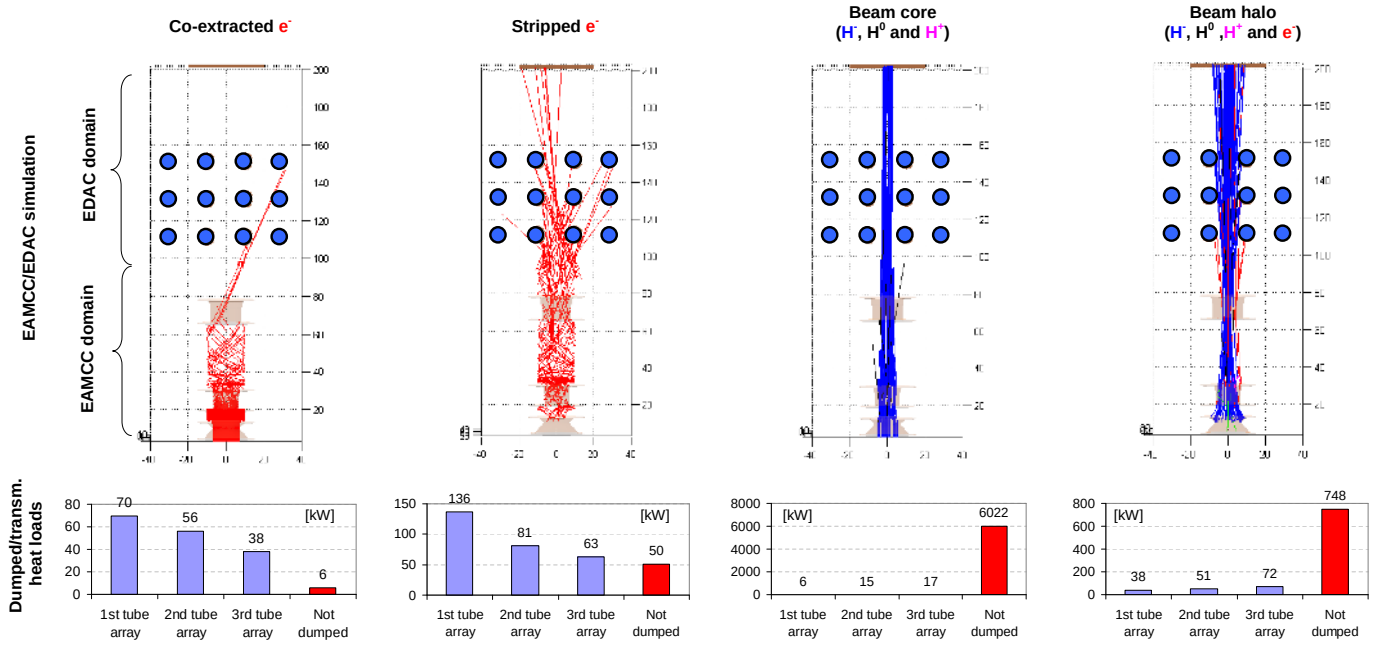

Figure 7: Heat loads dumped by the ED. The particle trajectories are simulated with EAMCC inside the accelerator and with EDAC in the ED area. The beam halo is considered to be given by H^- created on the PG downstream surface (plus related particles generated by stripping) and to have a power equal to 15% of the beam power.

~330 kW from stripped electrons (see Fig. 6). As co-extracted electrons are strongly deflected with respect to the aperture axis, the corresponding power can be almost completely dumped. On the other hand, stripped electrons present quite a high angular spread. Some of the trajectories are aligned with the aperture axis, so they cannot be dumped. Nevertheless, these electrons are mostly low energy ones, created by stripping reactions in the GG region, and so the corresponding load is relatively small.

Several different ED layouts have been investigated, considering different numbers of tube arrays (2,3 or 4) and diameters (8 or 10 mm). General indications are:

- the ED has to be located downstream of the GG;
- the closer the first array of tubes, the higher the load on it;
- the acceptable beamlet deflection tolerance (assumed to be 15 mrad according to the requirements) decreases if the tube diameter or increases the z position of the last tube array is increased;
- the load on the tubes is decreasing from the first to the last tube array. In order to maintain the load as uniform as possible, it is useful to enlarge the distance among the tube arrays. Nevertheless, there should be no open line-of-sight among the tubes.

After investigating several different layouts, an optimized ED design has been identified with three tube arrays at the positions z_1=110 mm, z_2=130 mm and z_3=150 mm (being z_{ref}=0 mm the position of PG upstream surface) and internal/external tube diameters of 6/8 mm (see Fig. 1).

With this configuration, the co-extracted and stripped e^- are found to be effectively dumped (only 56 kW are foreseen to pass through the ED, corresponding to about 11%), while 99% of the negative ion beam and 83% of the halo are transmitted (see Fig. 7). The beam halo is here considered to be given by H^- created on the PG downstream surface (plus related particles generated by stripping) and to have a power equal to 15% of the beam power. The halo is made of particles with much higher divergence angle than the beam core ($\theta_{RMS,halo} \sim 75$ mrad).

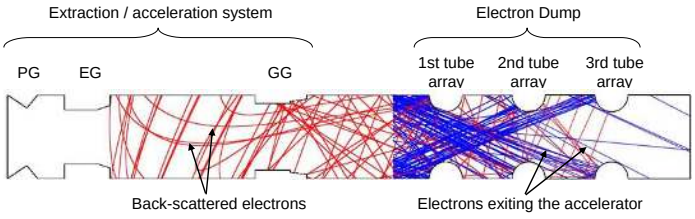

Figure 8: Electron backscattering simulation with the BACKSCAT code. The electrons exiting the accelerator are plotted in blue, the backscattered electrons in red.

The allowed horizontal deflection is ±27.4 mrad, calculated by considering the maximum deflection angle that makes the ion beamlet collide with the third array of tubes.

For simplicity of exposition, we implicitly assumed that the GG and the ED tube are firmly tied to the vessel ground reference; actually the GG may be connected to ground by a "spark damper circuitry", so that the application of a few tens of volts bias between the GG and the ED tubes is feasible and may be later considered for helping to control the secondary emission from ED tubes and the space charge compensation length.

Table 1: Dumped and transmitted power loads [kW] given by the co-extracted electrons, estimated with EDAC and BACKSCAT.

	EDAC	BACKSCAT (w/o scatt.)	BACKSCAT (with scatt.)
GG rear	0	0	18
1^{st} tube array	70	68	60
2^{nd} tube array	56	54	48
3^{rd} tube array	38	41	34
Not dumped	6	7	10
Total	170	170	170

Table 2: Dumped and transmitted power loads [kW] given by the stripped electrons, estimated with EDAC and BACKSCAT.

	EDAC	BACKSCAT (w/o scatt.)	BACKSCAT (with scatt.)
GG rear	0	0	33
1^{st} tube array	136	135	117
2^{nd} tube array	81	79	71
3^{rd} tube array	63	66	53
Not dumped	50	50	56
Total	330	330	330

6.2. Effect of backscattered electrons

In order to consider also the electrons bouncing off the electron dump tubes and the secondary electrons emitted from the tube surfaces, the BACKSCAT code has been developed at Consorzio RFX. This is a 2D code able to estimate the transmitted and dumped particle fluxes also taking into account the electron backscattering effect. In the application to the SPIDER case, the computational domain comprises the extraction/acceleration system and the electron dump; as in the EDAC code, the particles are imported from EAMCC and injected 20 mm downstream of the accelerator exit (see Fig. 8).

The assumptions on the physics of backscattering considered in BACKSCAT are analogous to the ones assumed in EAMCC. In particular, a model based on the work by P.F. Staub [50] has been considered for the generation of backscattering electrons on the ED tubes. The probability for an electron impinging on a pipe to be backscattered is expressed as a function of the incidence angle (between the particle trajectory and the surface normal) and the electron energy E_0.

$$\eta(\vartheta) = \eta_0 \exp(A_0(1 - \cos\vartheta)) \tag{2}$$

where A_0 is obtained by fitting experimental data as:

$$A_0 = \left[1 - \exp\left(-1.83E_0^{\frac{1}{4}}\right)\right] \ln\left(\frac{1}{\eta_0}\right) \tag{3}$$

E_0 (expressed in keV) is the particle energy and η_0 is the probability to be backscattered at normal incidence ($\vartheta = 0$). The value of η_0 depend mostly on the material and has only a slight dependence on E_0, so that in the simulations the fixed value $\eta_0 = 0.25$ has been used. This model also account for an energy loss of the primary electron on the impact point with respect to the backscattered electron energy (E_B), according to:

$$E_B = E_0 \left\{ \frac{1}{\gamma} \left[1 - \frac{70|\ln B_\vartheta|^4}{\ln\left(\frac{S}{P}\right)^{-\frac{1}{p}}} \right] \right\}^{\frac{1}{\alpha}} \tag{4}$$

with:

$$\gamma = 1 - \exp(-6|\ln B_\vartheta|^{-\frac{3}{2}}) \tag{5}$$

$$B_\vartheta = B_0 \exp[\tau(2 - \cos\vartheta - \cos\vartheta_2)] \tag{6}$$

$$S = \exp(70|\ln B_\vartheta|^4)^p \tag{7}$$

B_0,τ and p and α, obtained from fits of experimental data [51, 52], are respectively 0.27, 0.35, 0.27 and 2.2. P is a random number between 0 and 1 (assuming an uniform distribution) and ϑ_2 is the angle at which the particle is backscattered (with respect to the surface normal). Considering the hypothesis of isotropic backscattering (well justified in this energy range), ϑ_2 is assumed to have a random value in the interval $[-\pi/2; \pi/2]$ (also with an uniform distribution).

Tab. 1 (for co-extracted e^-) and Tab. 2 (for stripped e^-) show a good agreement between the EDAC and BACKSCAT codes if the backscattering in BACKSCAT is switched off. If this effect is switched on, a slightly lower heat load is obtained on the tubes, a slightly higher amount of electrons are estimated to escape from the ED and some heat load is also foreseen on the rear part of the GG.

7. Alignment and thermo-mechanical optimization

The alignment among the corresponding apertures of the first three grids (PG, EG and GG) is an important parameter for the optic quality of the ion beam exiting from the accelerator. For this reason, the in-plane deformation (along x and y axes) of these grids must be evaluated with good precision and in different operating scenarios.

7.1. Description of the ALIGN code

The ALIGN code, developed at Consorzio RFX, has the goal to calculate the horizontal displacement of the apertures, which is the most critical one (in fact the vertical displacement is always smaller). It is an analytical iterative code, which takes into account the variation of water and copper properties with temperature. Firstly, an equation can be written relating the heating power deposited on a grid segment and the heat carried away by cooling in steady state conditions:

$$P = \dot{m} \cdot C_{water} \cdot (T_{water,out} - T_{water,in}) \tag{8}$$

where P is the power deposited on a grid segment, $\dot{m}$ the cooling water flow on a segment, C_{water} the specific heat of water, $T_{water,in}$ and $T_{water,out}$ the inlet and outlet temperatures of the cooling water. The power P is estimated from experimental evaluations for the PG, with the EAMCC code for EG and GG,

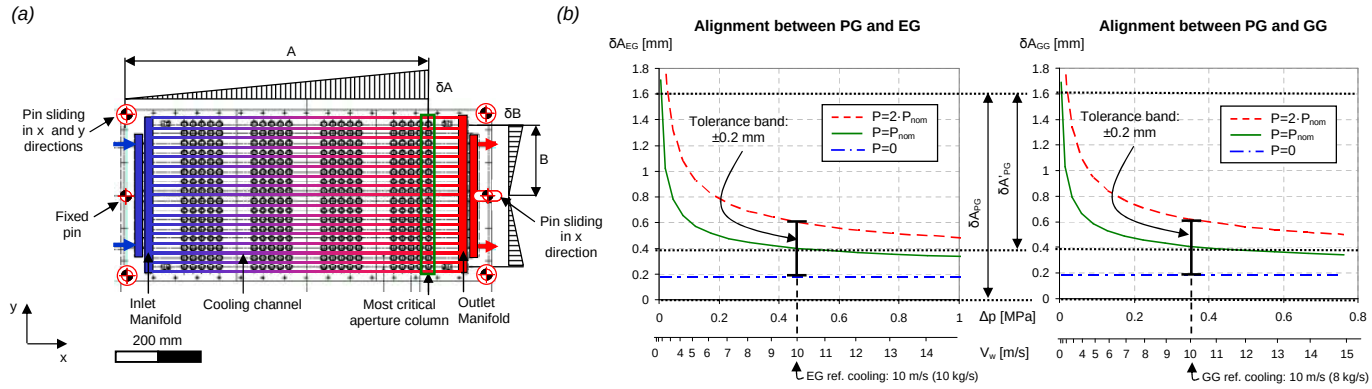

Figure 9: Alignment optimization for the grids: (a) Cooling and fixing scheme; (b) In-plane deformation plots, estimated with ALIGN, with identification of PG aperture pre-offset and of the minimum EG and GG cooling parameters (in terms of pressure drop, water velocity and water flow). The horizontal displacements δA (referred to the fixed pins) of the most critical aperture columns on the EG and GG are plotted as a function of the water pressure drop of the cooling water inside the two grids (and of the water velocity in the second scale). Three power scenarios are considered: with no power load, with the nominal power and with a power load corresponding to the double of the nominal value. The nominal power is the sum of the power given by the stripped and co-extracted electrons, as calculated by the EAMCC code in the reference operating scenario (full power and extracted e^-/H^- ratio equal to 1).

$T_{water,in}$ and $\dot{m}$ can be chosen, and C_{water} can be in first instance calculated as a function of $T_{water,in}$. Hence we can estimate the outlet water temperature as:

$$T_{water,out} = T_{water,in} + \frac{P}{\dot{m} \cdot C_{water}} \tag{9}$$

The average temperature of the cooling water is:

$$T_{water,av} = \frac{T_{water,in} + T_{water,out}}{2} = T_{water,in} + \frac{P}{2 \cdot \dot{m} \cdot C_{water}} \tag{10}$$

The heating power deposited on a grid segment can be written also as a function of the heat exchange parameters:

$$P = q_{av} \cdot A_{exchange} \tag{11}$$

where q_{av} is the average power density exchanged between water and copper, while $A_{exchange}$ is the total interface area between water and copper, where there can be heat exchange. $A_{exchange}$ can be calculated as the sum of the lateral walls of the cooling channels and the manifolds. q_{av} is a function of the Convective Heat Transfer (CHT) coefficient α and the difference between wall and water temperature.

$$q_{av} = \alpha_{av} \cdot (T_{wall,av} - T_{water,av}) \tag{12}$$

The average CHT coefficient α_{av} can be estimated with the Sieder-Tate correlation [53]:

$$\begin{aligned} \alpha_{av} &= Nu_{t,av} \cdot \frac{\lambda}{D_h} \\ &= 0.027 \cdot Re_{av}^{0.8} \cdot Pr_{av}^{\frac{1}{3}} \cdot \frac{\lambda}{D_h} \end{aligned} \tag{13}$$

where Re_{av} is the average Reynolds number, Pr_{av} the average Prandtl number, λ the thermal conductance of the fluid and D_h the channel hydraulic diameter.

Hence, by inverting equation (12) we can calculate $T_{wall,av}$ as:

$$T_{wall,av} = T_{water,av} + \frac{q_{av}}{\alpha_{av}} \tag{14}$$

where $q_{av} = \frac{P}{A_{exchange}}$ (inverse of Eq. (11)) and α_{av} is estimated with equation (13).

The thermal conductance of copper is very high, compared with the water/copper interface conductance:

$$\frac{\frac{\lambda_{Cu} \cdot A_{grid}}{s}}{\alpha_{av} \cdot A_{exchange}} > 20 \tag{15}$$

where λ_{Cu} is the thermal conductance of copper, A_{grid} is the area of a grid side (taken equal to 0.3 m^2), s is a typical copper layer thickness (taken equal to 1 mm), α_{av} is a typical CHT coefficient for these applications (taken equal to 50000 W/(K · m^2) and $A_{exchange}$ is the water/copper heat exchange area (taken equal to 0.1 m^2).

Hence, the average grid temperature can be assumed to be equal to the average temperature of the wall channels:

$$T_{grid,av} = T_{wall,av} \tag{16}$$

This hypothesis is confirmed by detailed thermo-structural models [54], using both the approaches based on Finite Elements Method (FEM) and on Computational Fluid Dynamics (CFD).

Summarizing in a single equation all the evaluations made, we can write $T_{grid,av}$ as a function of known parameters:

$$T_{grid,av} = T_{water,in} + \frac{P}{2 \cdot \dot{m} \cdot C_{water}} + \frac{P}{A_{exchange} \cdot 0.027 \cdot Re_{av}^{0.8} \cdot Pr_{av}^{\frac{1}{3}} \cdot \frac{\lambda}{D_h}} \tag{17}$$

For a better approximation, this equation can be applied iteratively, in order to set the water properties as a function of $T_{water,av}$.

In the ALIGN code, to estimate the maximum effect of heating on beam deviation, we calculate the aperture displacement δA (referred to the most critical aperture column highlighted in Fig. 9a), considering the linear thermal expansion of the grid:

$$\delta A_{PG} = \gamma_{Cu} \cdot A_{PG} \cdot (T_{average,PG} - T_{ref}) \tag{18}$$

$$\delta A_{EG} = \gamma_{Cu} \cdot A_{EG} \cdot (T_{average,EG} - T_{ref}) \tag{19}$$

$$\delta A_{GG} = \gamma_{Cu} \cdot A_{GG} \cdot (T_{average,GG} - T_{ref}) \tag{20}$$

where the three $T_{average}$ are the average temperatures of the first three grids, γ_{Cu} is the thermal expansion coefficient, A_{PG}, A_{EG} and A_{GG} are the maximum horizontal distance of apertures from the fixed pin (see Fig. 9a) and T_{ref} is the reference temperature for manufacturing (fixed at 20 °C).

The parameters calculated with the ALIGN code (in particular, the in-plane deformation of the grids) are almost identical to those calculated with more detailed numerical models (see Par. 7.3), confirming that the hypotheses made are consistent and the code reliable.

7.2. Alignment optimization

Optimized parameters for the cooling of the SPIDER grids, calculated with the ALIGN code, are reported in Fig. 9b. With a reasonable water flow (0.74 kg/s for PG, 10 kg/s for EG and 8 kg/s for GG) it is possible to guarantee a good alignment among grids (misalignment lower than 0.2 mm, corresponding to about 2 mrad deflection) in a power range between zero and two times the nominal power (estimated with EAMCC) for both the grids. Higher water flows can meet the requirements on alignment in a larger range of power loads, but could be an issue for the corrosion/erosion of the channels and manifolds. This is to be tested in the ICE (Insulation Cooling Experiment) facility [55].

7.3. Thermo-mechanical simulations of the accelerator

The alignment requirements are the most critical ones and impose the minimum cooling flow in the grids. Other requirements come from temperature, stress, fatigue life and out-of-plane deformation. In order to check these points, a finite element model in ANSYS, with two cooling channels and the whole width of the grids, has been considered for the EG and GG. This has permitted to optimize the geometry and shape of the cooling channels in order to fulfil several different requirements:

- A peak temperature on the grids as low as possible, and in any case lower than 300 °C (beyond this temperature the copper thermo-mechanical properties are sensibly worsened than at room temperature);
- Stress peaks as low as possible, and in any case satisfying the ITER SDC-IC (Structural Design Criteria for In-Vessel Components) criteria [56];
- Fatigue life (depending on strain peaks) as long as possible.

The grids have to withstand two categories of stresses:

- Cyclic thermal stress due to the temperature gradients between hotter and colder zones. These stresses must be maintained low in order to satisfy the requirement on fatigue life;
- Static stress due to the water pressure. The local values of equivalent stress must be lower than the allowable values for electrodeposited copper (fixed at 100 MPa).

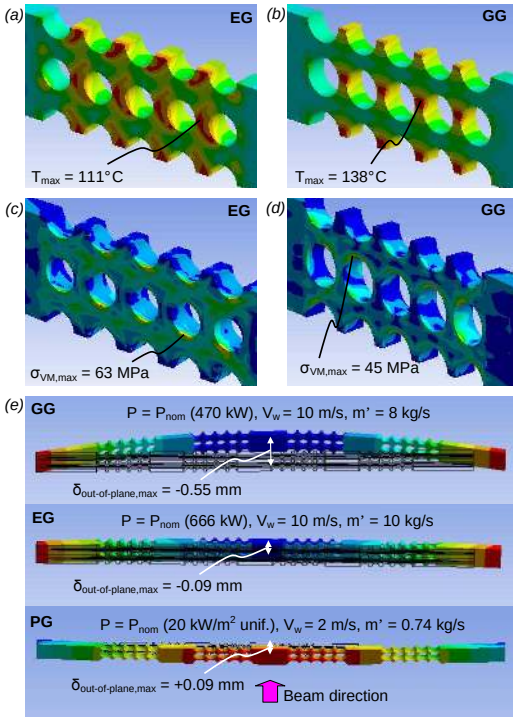

Figure 10: Main results of the thermo-structural analyses on the grids performed with the ANSYS code considering the reference scenario: maximum temperature (a) on the EG and (b) on the GG; maximum Von Mises equivalent stress (c) on the EG and (d) on the GG; (e) Out-of-plane deformations of the three grids. The PG temperature and stress plots are not shown, because the temperature is uniform and the stress almost null.

The position and dimensions of the cooling channels, as well as the water flow, have been optimized in order to satisfy the structural, ratcheting and fatigue verifications according to the ITER SDC-IC criteria, and at the same time to have low out-of-plane deformations of the grids. Therefore several analyses have been performed to estimate the temperatures, stresses and deformation along the grids in different operating scenarios. The thermo mechanical analyses have required a non linear elastoplastic model, taking into account the kinematic hardening for the material, while the copper properties are taken from the ITER Material Handbook [57].

The main outputs are presented in Fig. 10, showing acceptable results and in particular a very low out-of-plane deformation of the EG (less than a tenth of millimeter), which represents an important aspect for beam optics.

7.4. Electron dump engineering proposal

A viable engineering proposal of the ED cooling system has been developed, suitable for removing the expected power load and compliant with the layout constraints. The first array of tubes, which is the most heated, has been taken into consideration for the cooling parameters' choice. An analytical iterative model (similar to ALIGN) has been used (with water and copper properties as a function of temperature), where the main relations used are Eqs. (10), (13) and (17).

The main design guidelines for the SPIDER ED are:

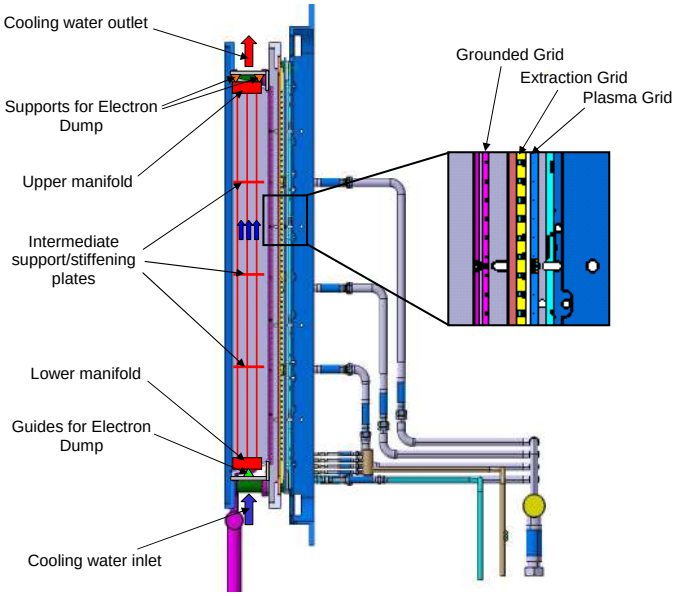

Figure 11: Electron dump engineering proposal.

- to obtain a thermal expansion of ED similar to that of the grids;
- to ensure easy manufacturing, assembly and disassembly.

A scheme of the proposal is reported in Fig. 11. Three arrays of 32 tubes each (with external diameter 8 mm, internal diameter 6 mm) run in parallel between an inlet manifold (at the bottom) and an outlet manifold (at the top).The ED supports (on the top) and guides (on the bottom) permit thermal deformations without stress (isostatic constraints) and good alignment with GG.

The GG support frame has been modified in order to leave sufficient room for the inlet and outlet manifolds. The tubes are welded to the inlet and outlet manifolds, and pass through five intermediate supports plates that increase the stiffness of the system. The cooling water is fed by means of two inlet manifolds and two outlet manifolds that pass through the bottom of the vacuum vessel.

7.5. Thermo-mechanical analysis of the electron dump tubes

The thermo-mechanical behaviour of the electron dump tubes is preliminary investigated by considering:

- A 0.3 kg/s water flow per tube, with a 10.6 m/s water velocity. The corresponding total flow on the whole ED is about 30 kg/s and the pressure drop about 0.5 MPa; both these parameters are compatible with the cooling plant requirements.
- An inlet water temperature of 35 °C (same as for EG and GG).
- 400 mm tube length, which is the distance between two "intermediate support/stiffening plates"

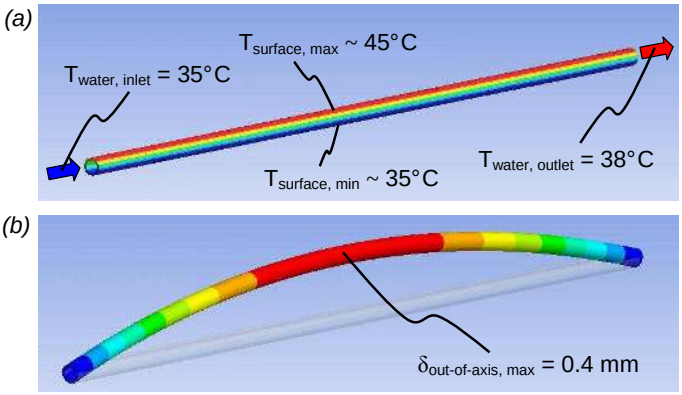

Figure 12: Thermo-mechanical analysis of the ED tubes, in the case of copper: (a) Temperature distribution, (b) Maximum out-of-axis deformation. The conservative hypothesis of free rotation at the edges is considered.

Table 3: Comparison between copper and stainless steel tubes.

	Cu tubes	SS tubes	Ratio
Max. temperature [°C]	45	73	
In axis deform. [*mm*]	0.15	0.23	1.5
Out of axis deform. [*mm*]	0.4	1.5	3.7

- Heat loads corresponding to the first array of ED tubes, uniformly applied to the front side (180° angle). The hypothesis of an uniform heat load is confirmed by the EDAC results.
- Free rotation at sides (conservative hypothesis)
- Free elongation (one edge fixed position and the other sliding along tube axis)
- Two options have been studied with tubes respectively made of copper and of stainless steel.

The main results obtained with copper tubes are shown in Fig. 12, while a comparison between the solutions with copper and stainless steel tubes is reported in Tab. 3. The out-of-axis deformation is to be considered the most critical parameter, because an excessive deformation can move the tubes close to the negative ion beamlets, with possible serious damages. Nevertheless, as the heat load comes mainly from the upstream side, the deformation of the ED tubes is expected to be mainly in the direction of the GG. In this regard, it can be noted that copper tubes have a much better behaviour than stainless steel ones. In particular, the maximum temperature reached at the tube surface is lower (copper is an optimal heat sink) and as a consequence also the out-of-axis deformation is lower (less than one third). On the other hand, the manufacturing process is foreseen to be easier and cheaper with stainless steel tubes.

Due to its great advantages in terms of out-of-axis deformation, the solution with copper tubes has been chosen. The assessment of the most suitable bonding process between the tubes and the manifolds is currently on-going.

8. Conclusions

The design of the extraction and acceleration system for the SPIDER experimental device has been accomplished by taking into account at the same time physics and engineering requirements. Many aspects of the design have been improved with respect to the 2008 design, using a comprehensive set of analytical and numerical codes whose results have been discussed in several meetings during the last two years.

The main guideline, applied to all the relevant aspects of the machine, have been to obtain a versatile design, according to the "robust design" philosophy, able to cope with possible expected and unexpected variations in the operating parameters.

In particular, the following improvements have been introduced:

- The magnetic configuration has been modified in order to permit a suitable magnetic compensation of the vertical ripple due to the suppression field. This has been done by adding compensation magnets and ferromagnetic material on the GG.
- A mechanical offset of the grid apertures has been introduced to compensate for the repulsion among beamlets and for the thermal deformations of the three grids.
- The position and shape of the cooling channels and magnets on the grids have been optimized in order to decrease the out-of-plane deformation, especially of the EG.
- An electron dump has been added to dispose of the electrons exiting from the accelerator; this component is designed in compliance with the layout constraints given by the other components and by the diagnostic line-of-sights.

Several conditions will be investigated during the experimental campaigns, like the the plasma source conditioning, the effect of the caesium inside the beam source, the operating temperature of the PG etc. For this reason, the most flexible solutions have been adopted in order to allow possible modifications and further optimization during the experimental phase.

Acknowledgements

The authors would like to thank Dr. H.P.L. de Esch, Dr. G. Fubiani, Dr. L. Grisham, Dr. R.S. Hemsworth and Dr. M.J. Singh for the support and the fruitful discussions.

This work was set up in collaboration and financial support of Fusion for Energy.

References

References

[1] R. Hemsworth, et al., Status of the ITER heating neutral beam system, Nucl. Fusion 49 (2009) 045006.
[2] T. Inoue, et al., Design of neutral beam system for ITER-FEAT, Fus. Eng. and Design 56-57 (2001) 517-521.
[3] E. Speth, et al., Overview of the RF source development programme at IPP Garching, Nucl. Fusion 46 (2006) S220-S238.
[4] P. Franzen, et al., Physical and experimental background of the design of the ELISE test facility, AIP Conf. Proc. 1097 (2009) 451.
[5] U. Fantz, et al., Physical performance analysis and progress of the development of the negative ion RF source for the ITER NBI system, Nucl. Fusion 49 (2009) 125007.
[6] A. Stäbler, et al., Development of a RF-driven ion source for the ITER NBI system, Fus. Eng. and Design 84 (2009) 265-268.
[7] P. Sonato, et al., The ITER full size plasma source device design, Fusion Eng. Des. 84 (2009) 269.
[8] D. Marcuzzi, et al.,Detail design of the beam source for the SPIDER experiment, Fusion Eng. Des. 85 (2010) 1792.
[9] P. Agostinetti, et al., Design of a low voltage, high current extraction system for the ITER Ion Source, AIP Conf. Proc. 1097 (2009) 325.
[10] M.J. Singh and H.P.L. De Esch, Physics design of a 100 keV acceleration grid system for the diagnostic neutral beam for international tokamak experimental reactor, Rev. Sci. Instrum. 81, 013305 (2010).
[11] B. Heinemann, et al., Design of the half-size ITER neutral beam source test facility ELISE, Fusion Eng. Des. 84 (2009) 915.
[12] P. Agostinetti, et al., Optimisation of the magnetic field configuration for the negative ion source of ITER neutral beam injectors, 18th International Toki Conference on Development of Physics and Technology of Stellarators/Heliotrons en route to Demo, Ceratopia Toki, Japan, 2008. http://www.nifs.ac.jp/itc/itc18/ITC18upload.html
[13] A. Rizzolo, et al., Design and analyses of a one-dimensional CFC calorimeter for SPIDER beam characterization, Fusion Eng. Des. 85 (2010) 2268.
[14] J. Pamela, A model for negative ion extraction and comparison of negative ion optics calculations to experimental results. Rev. Sci. Inst. 62 (1991) 1163.
[15] W.B. Hermannsfeld, Electron Trajectory Program, SLAC report, Stanford Linear Accelerator Center, SLAC-226 (1979).
[16] H.P.L. de Esch, R.S. Hemsworth and P. Massmann. Updated physics design ITER-SINGAP accelerator. Fusion Eng. Des. 73 (2005) 329.
[17] H.P.L. De Esch, Personal communication and support (2007), Association EURATOM-CEA, CEA-Cadarache, St. Paul-Lez-Durance, France.
[18] K. Jousten, Wutz Handbuch Vakuumtechnik - theorie und praxis, 9th edition, Vieweg und Teubner Verlag, Wiesbaden (2006), ISBN-13 978-3-8348-0133-3
[19] U. Fantz, et al., Spectroscopy - a powerful diagnostic tool in source development, Nucl. Fusion 46 (2006) S297-S306.
[20] E.W. Thomas, Oak Ridge National Laboratory, Technical Report No. ORNL-6088, 1985.
[21] L. Svensson, SRD-53-PR, -MI, -MP, -SI, -SP (NEUTRAL BEAM TEST FACILITY), Version 1.2, IDM UID 2WCCSG, October 2009.
[22] M.S. Phadke, Quality Engineering Using Robust Design. Prentice Hall, 1989.
[23] M. Cavenago, et al., Development of Small Multiaperture Negative Ion Beam Sources and Related Simulation Tools, , AIP Conf. Proc. 1097 (2009) 149.
[24] P. Agostinetti, et al., Compensation of beamlet deflection by mechanical offset of the grids apertures in the SPIDER ion source, IEEE Trans. Plasma Sci., 38 (7) 1579-1583 (2010).
[25] OPERA-3D, Vector Fields Co.Ltd., http://www.vectorfields.com/
[26] N. Pilan, et al., IRES: a code evaluating the beamlet beamlet interaction for multi-aperture electrostatic accelerators, IEEE Trans. Plasma Sci., 38 (6) 1478-1481 (2010).
[27] P. Spädtke, Numerical simulations of ion beam related problems, Rev. Sci. Instrum. 63 (4), 2647 (1992).
[28] H. Wituschek, et al., Investigations of extraction systems with low aberrations, Rev. Sci. Instrum. 63 (4), 2785 (1992).
[29] A. J. T. Holmes, et al., Beam steering in tetrode extraction systems, Rev. Sci. Instrum. 52, 172 (1981).
[30] T. Inoue, et al., Recent progress on high power negative ion sources at JAERI, Plasma Devices and Operations 3, 211 (1994).
[31] M. Kashiwagi, et al., Compensation of beamlet repulsion in a large negative ion source with a multi aperture accelerator, AIP Conf. Proc. 1097 (2009) 421.
[32] Y. Fujiwara, et al., Beamlet-beamlet interaction in a multi-aperture negative ion source, Rev. Sci. Instrum. 71 (8), 3059 (2000).
[33] M. Kamada, et. al., Beamlet deflection due to beamlet-beamlet interaction in a large-area multiaperture negative ion source for JT-60U, Rev. Sci.

Instrum., 79, 02C114 (2008).
[34] Y. Takeiri, et al., Negative hydrogen ion source development for large helical device neutral beam injector, Rev. Sci. Instrum. 71 (2), 1225 (2000).
[35] Y. Takeiri, et al., Multibeamlet focusing of intense negative ion beams by an aperture displacement technique, Rev. Sci. Instrum., 66, 5236-5243 (1995).
[36] M. Tanaka, et al., Investigation of beam deflection reduction and multibeamlet focus at a large-area negative ion source for a neutral beam injector with 3-D beam trajectory simulation, Nuclear Instruments and Methods in Physics Research A 449, 22 (2000).
[37] M. Hamabe, et al., Compensation of beam deflection due to the magnetic field using beam steering by aperture displacement technique in the multibeamlet negative ion source, Rev. Sci. Instrum., 72, 3237-3244 (2001).
[38] G. Fubiani, et al., Modeling of secondary emission processes in the negative ion based electrostatic accelerator of the International Thermonuclear Experimental Reactor. Phys. Rev. Special Topics Accelerators and Beams 11, 014202 (2008).
[39] G. Fubiani, et al., Analysis of the two accelerator concepts foreseen for the neutral beam injector of the International Thermonuclear Experimental Reactor. Phys. Rev. Special Topics Accelerators and Beams 12, 050102 (2009).
[40] W. Kraus, et al., Long pulse H^- beam extraction with a rf driven ion source with low fraction of co-extracted electrons, AIP Conf. Proc. 1097 (2009) 257.
[41] W. Kraus, et al., Long pulse H^- beam extraction with a rf driven ion source on a high power level, Rev. Sci. Instrum. 81, 02B110 (2010).
[42] M. Cavenago, et al., Negative ion extraction with finite element solvers and ray maps, IEEE Trans. Plasma Sci., 36 (4) 1581-1588 (2008).
[43] N. Marconato, et al., Simulation, Code Benchmarking and Optimization of the Magnetic Field Configuration in a Negative Ion Accelerator, Fusion Eng. Des. (2011), doi:10.1016/j.fusengdes.2011.01.052.
[44] ANSYS Manual, ANSYS Inc., http://www.ansys.com/
[45] COMSOL Manual, COMSOL AB http://www.comsol.com/
[46] PerMag Manual, private communication from D. Ciric (2007), UKAEA Fusion/Euratom Association, Culham Science Centre, Abingdon, United Kingdom.
[47] A. T. Forrester, Large Ion Beams: Fundamentals of Generation and Propagation, Wiley-Interscience (1988).
[48] H.P.L. De Esch and R.S. Hemsworth, Dealing with post-accelerated electrons in the ITER SINGAP accelerator, Fusion Eng. Des. 82 (2007) 723.
[49] H.P.L. de Esch and M.J. Singh, Electron dumps for ITER HNB and DNB beamlines, Fusion Eng. Des. 85 (2010) 707.
[50] P. F. Staub, Bulk target backscattering coefficient and energy distribution of 0.5-100 keV electrons: an empirical and synthetic study, J. Phys. D: Appl. Phys. 27 1533 (1994)
[51] T. Matsukawa, et al., Measurements of the energy distribution of backscattered kilovolt electrons with a spherical retarding-field energy analyser, J. Phys. D: Appl. Phys. 7 695 (1974)
[52] E. J. Sternglass, Backscattering of Kilovolt Electrons from Solids, Phys. Rev. 95, 345358 (1954).
[53] J.H. Lienhard IV and J.H. Lienhard V. A Heat Transfer Handbook, third ed., Phlogiston Press (2003).
[54] P. Agostinetti, Methods for the Thermo-mechanical Analysis and Design of High Power Ion Beam Sources, Ph.D. Thesis, University of Padua, 2008.
[55] O. Barana, et al., Analysis of the Control System of ICE, the Insulation and Cooling Test Facility for the Development of the ITER Neutral Beam Injector, 12^{th} International Conference of Accelerator and Large Experimental Physics Control Systems, Kobe, Japan, 2009 http://accelconf.web.cern.ch/accelconf/icalepcs2009/papers/wep062.pdf
[56] ITER SDC-IC, Structural Design Criteria for ITER In-Vessel Components. ITER Document No. G 74 MA 8 (2004) (internal project document distributed to the ITER participants).
[57] ITER MPH, Material Properties Handbook. ITER Document No. G 74 MA 16 (2006) (internal project document distributed to the ITER participants).